



PCCP

Turing patterns on radially growing domains: Experiments and simulations

Journal:	<i>Physical Chemistry Chemical Physics</i>
Manuscript ID	CP-ART-12-2018-007797.R1
Article Type:	Paper
Date Submitted by the Author:	25-Feb-2019
Complete List of Authors:	Konow, Christopher; Brandeis University, Department of Chemistry Somberg, Noah; Brandeis University, Chemistry Department Chavez, Jocelyne; New Mexico State University, Department of Chemistry and Biochemistry Epstein, Irving; Brandeis University, Chemistry Dolnik, Milos; Brandeis University, Chemistry Department

SCHOLARONE™
Manuscripts

Cite this: DOI: 10.1039/xxxxxxxxxx

Turing patterns on radially growing domains: Experiments and simulations[†]

 Christopher Konow,^a Noah H Somberg,^a Jocelyne Chavez,^b Irving R Epstein^a and Miloš Dolník^{*a}

Received Date

Accepted Date

DOI: 10.1039/xxxxxxxxxx

www.rsc.org/journalname

We study Turing pattern formation in a system undergoing radial growth in two dimensions. The photosensitive chlorine dioxide-iodine-malonic acid reaction is illuminated to inhibit patterning, with a growing non-illuminated circular domain in which the pattern develops. We examine the relationship between the linear radial growth rate and the resulting pattern morphology. Faster growth causes the pattern to form parallel to the growing boundary as concentric rings, while slower growth leads to pattern formation perpendicular to the growing boundary. We observe three distinct growth modes for the Turing patterns, which also depend on the radial growth rate. The experimental results are qualitatively reproduced in numerical simulations using the Lengyel-Epstein model with an additional term to account for the photosensitivity of the reaction. These results may provide new insight into how patterns form in growing biological systems.

1 Introduction

Over sixty years ago, Alan Turing proposed a mechanism for the spontaneous generation of heterogeneity in an originally homogeneous system *via* chemical reaction and diffusion.¹ This mechanism can result in temporally stable, spatially periodic patterns which are commonly referred to as Turing patterns.^{2,3} Morphologically, these patterns are characterized by stripes or hexagonal arrays of spots with a characteristic wavelength.^{4,5} In nature, there are many systems for which patterning is thought to arise from a Turing-type mechanism^{6,7}, such as fish skins^{7–9}, bird feathers^{10,11}, leopard coats^{12,13}, seashells⁷, and biomass distributions in arid ecosystems.^{14,15}

Despite the wide variety of Turing patterns found in nature, experimental studies on Turing pattern-generating systems remain difficult due to the inherent complexity of biological processes.^{2,6,13} With the introduction of the continuously fed unstirred reactor (CFUR) in the late 1980s,¹⁶ chemical systems have often been used as viable alternatives to study Turing pattern behavior due to their more well-understood dynamics.^{2,17,18} In particular, the chlorite-iodide-malonic acid (CIMA) reaction^{2,3} and its derivative, the chlorine dioxide-iodine-malonic acid (CDIMA) reaction,^{19–24} have been used for the past three decades to gain

deeper insight into the dynamics of Turing pattern formation. One particular advantage of using the CDIMA system is the reaction's photosensitivity.¹⁹ When exposed to intense visible light, the Turing pattern is inhibited due to the photodissociation of molecular iodine.¹⁹ This property has previously been used to explore the effect of spatiotemporal forcing of Turing patterns^{23,24} as well as pattern recovery after a period of inhibition²⁰.

However, most prior studies on Turing patterns in chemical systems ignore a critical aspect of biological systems: growth. Growth has been shown to significantly impact biological pattern formation.^{8,9,12,13,25} In addition, mathematical simulations reveal a wealth of new Turing pattern phenomena arising when growth is included, such as the widening of the region in parameter space where Turing patterns exist,^{26–28} history dependence of the resulting pattern,²⁸ patterns on periodically deforming domains,²⁷ and patterns arising from activator-activator and short range inhibitor-long range activator systems.²⁶ Míguez *et al.* have performed the only experimental studies on the effect of growth, specifically one-dimensional axial growth, on a Turing pattern resulting from the CDIMA reaction.²¹ They find that the growth rate has a significant impact on the pattern orientation, with faster speeds orienting the pattern parallel and slower speeds orienting the pattern perpendicularly with respect to the moving boundary.²¹

In this article, we examine the impact of two-dimensional domain growth on Turing pattern development. We present an experimental method for controlling the two-dimensional growth of Turing patterns generated by the CDIMA reaction. Both experimental and numerically simulated results of linear (constant)

^a Department of Chemistry, MS 015, Brandeis University, Waltham, MA 02454, USA. E-mail: dolnik@brandeis.edu

^b Department of Chemistry and Biochemistry, MSC 3C, P.O. Box 30001, New Mexico State University, Las Cruces, NM 88003-8001, USA.

[†] Electronic Supplementary Information (ESI) available: Videos of the growth of Turing patterns leading to different final pattern morphologies (both experimental and simulated) mentioned in the text. See DOI: 10.1039/cXCP00000x/

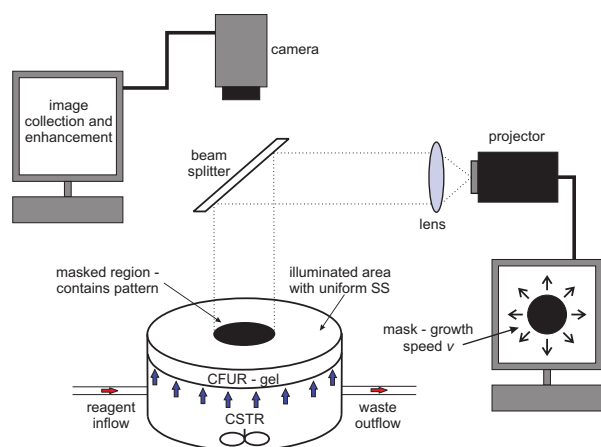


Fig. 1 Schematic of experimental setup for generating Turing patterns in the CDIMA reaction with radially growing domain. The blue arrows indicate the one-sided reagent inflow to the CFUR.

radial growth of a domain with Turing patterns show good agreement with the experiments performed by Míguez *et al.*,²¹ and extend them into the second dimension. We observe three distinct modes of Turing pattern formation in growing domains and provide some discussion of how the growth mode relates to the final pattern. To analyze the stability and robustness of the various Turing pattern modes, we construct a parametric diagram from numerical simulations and discuss the size of the various patterning regions. To conclude, we consider other studies that might be performed on two-dimensional Turing patterns in growing domains, some of which are currently in progress.

2 Methods

2.1 Experimental

2.1.1 Apparatus and Procedure

A schematic overview of the experimental setup is depicted in Figure 1. The experiments were carried out in a CFUR composed of a 2% agarose gel (Sigma-Aldrich, thickness 0.45 mm, diameter 25 mm). The CFUR gel was fed on one side with well-mixed reagents from a continuously stirred tank reactor (CSTR, volume 2.0 mL, stir rate 660 rpm). The CSTR and CFUR were separated by two membranes, a cellulose nitrate membrane (Whatman, pore size 0.45 μm) and an anapore membrane (Whatman, pore size 0.2 μm), both of which were impregnated with 2% agarose gel to provide rigid support and color contrast with the gel.

Three reagent solutions were fed into the CSTR using peristaltic pumps (Gilson). First, an unforced Turing pattern was allowed to develop under ambient light (0.4 mW cm^{-2}) until the pattern was fully formed, which took approximately 3 hours. Then, a MATLAB-controlled program was used to generate a growing mask, where the growing domain was a dark circle under ambient light (0.4 mW cm^{-2}) on a visible light background (10.1 mW cm^{-2}). This inhibited the patterns outside of the growing mask by forcing the reaction in that region of the CFUR into the light steady state (SS).¹⁹ The mask was projected onto the CFUR using a PC-controlled DLP-projector (Dell 1510X). Images of the pat-

terns were collected with a CCD Monochrome Imaging Camera (PixeLINK, PL-B953U). Images were collected every minute over the course of the experiment, which typically lasted from one to three days. At the conclusion of the experiment, the resulting images were enhanced to improve contrast using Corel Photo-Paint x5. MATLAB was used to develop space-time plots and Adobe Photoshop was used to create the animations found in the ESI†.

2.1.2 Materials

The CSTR was fed with the following three solutions: (i) I_2 (Aldrich) and acetic acid (Fisher, 10% by volume, used to fully dissolve iodine); (ii) malonic acid (MA, Aldrich) and poly-(vinyl alcohol) (PVA, Aldrich, Mw 9,000-10,000, 80% hydrolysed); and (iii) ClO_2 , which was prepared according to ref. 29. All three infeed solutions also contained 10 mM H_2SO_4 (Aldrich). The initial concentrations of the reactants in the CSTR (after mixing the three solutions as they entered the CSTR) for all experiments were: $[\text{I}_2] = 0.4 \text{ mM}$, $[\text{MA}] = 1.0 \text{ mM}$, $[\text{ClO}_2] = 0.08 \text{ mM}$, and $[\text{PVA}] = 10 \text{ g L}^{-1}$. Concentrations of the stock I_2 and ClO_2 solutions were measured spectrophotometrically using a Shimadzu UV-Visible Spectrophotometer (UV-1650PC).

2.2 Numerical Simulations

We simulated the CDIMA reaction using the Lengyel-Epstein two-variable model³ modified to account for the effects of illumination.¹⁹

$$\frac{\partial u}{\partial \tau} = a - u - \frac{4uv}{1+u^2} - W + \nabla^2 u \quad (1)$$

$$\frac{\partial v}{\partial \tau} = \sigma \left[b \left(u - \frac{uv}{1+u^2} + W \right) + d \nabla^2 v \right] \quad (2)$$

Here, u and v are dimensionless concentrations of the activator and inhibitor species, I^- and ClO_2^- respectively. a , b , d , and σ are dimensionless parameters, and W is the dimensionless effect of the illumination. For our simulations the parameters were fixed at $a = 12$, $d = 1$, and $\sigma = 50$. We used $W = 1.5$ to simulate the illuminated area and $W = 0$ to simulate the dark area of the reactor. The parameter b was varied between 0.300 and 0.340, and the growth rate of the dark domain was varied between 0.05 and 0.75 s.u./t.u. (dimensionless space units per time unit).

Equations 1 and 2 were solved numerically using COMSOL Multiphysics versions 4.4 and 5.3, with zero-flux boundary conditions along the circular boundary of the reactor. The size of the dark area of the reactor was increased stepwise *via* parametric sweep of the radius by varying increments depending on the growth rate. The time-dependent solver was fixed to solve at $t = 0$ and $t = 10$ t.u. for each radius step. Each simulation was run until a final radius of 100 s.u.

3 Results and Discussion

3.1 Final Pattern Morphologies

We observe a distinct trend for the resulting pattern morphologies from two-dimensional radial growth. For fast growth rates, stripes in the shape of concentric rings form parallel to the growing boundary, as seen in Figure 2a for a radial growth rate of 0.50 mm/h. For slow growth rates, the resulting Turing stripes

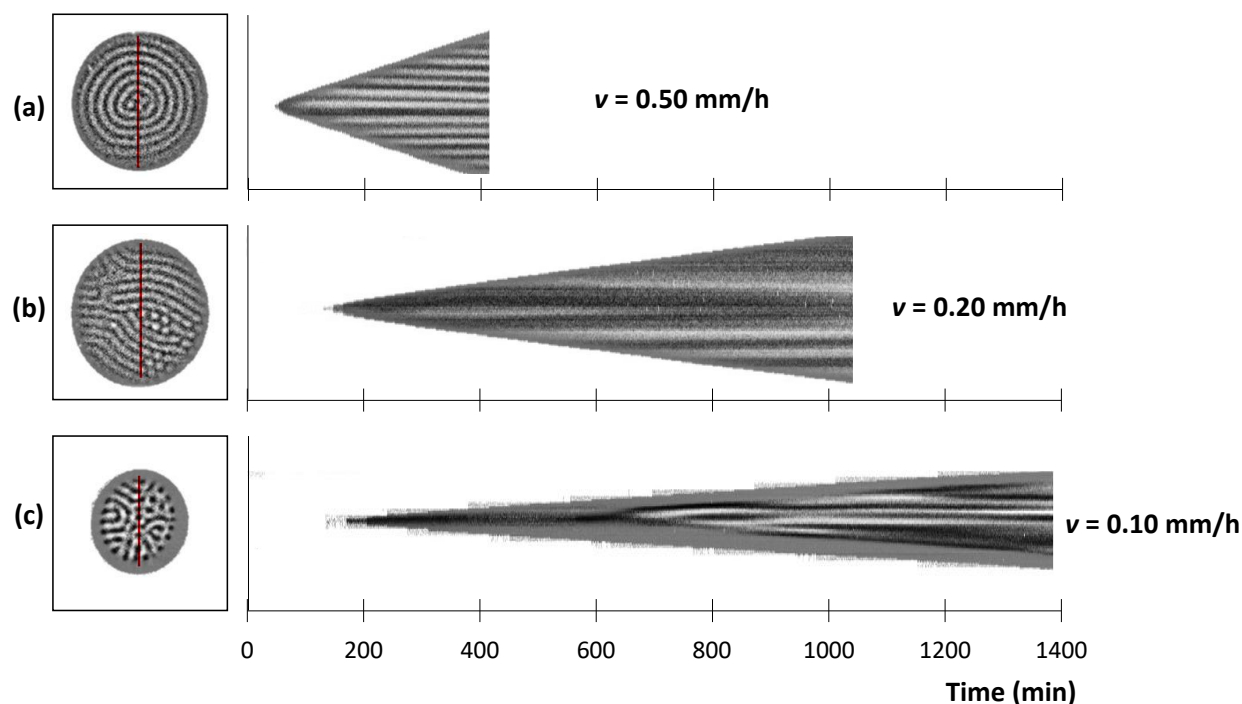


Fig. 2 Turing patterns on a radially growing domain for fast, intermediate, and slow growth rates. Final Turing pattern (left) and a space-time plot of the experiment (right) are shown. Each box around the final Turing patterns is 7.66 mm \times 7.66 mm. The red lines indicate the location where the space-time plot information was taken. Radial growth rates (total growth time) are (a) 0.50 mm/h (416 min), (b) 0.20 mm/h (1041 min), and (c) 0.10 mm/h (1386 min).

are oriented perpendicular to the the growing boundary, as seen in Figure 2c for a growth rate of 0.10 mm/h. Note that there are also areas of inverted spots (black hexagonal spots with white borders) in Figure 2c. This is due to experimental irregularities such as slight inhomogeneities in the CFUR gel. However, no concentric ring patterns are observed at the slower growth rates.

For intermediate growth rates (typically rates between 0.35 and 0.15 mm/h) we observe a striped pattern that is intermediate between concentric rings and perpendicular patterns. The stripes are oriented across the circular growing domain, similar to the perpendicular patterns. However, instead of extending radially from the center of the domain in many different directions, the stripes form parallel to one another, with most of the stripes growing in the same direction. An example of this type of pattern is shown in Figure 2b for a growth rate of 0.20 mm/h. These similarly-oriented stripes indicate the transition between the striped concentric rings and the perpendicular patterns shown in Figure 2a,c respectively. For all of the patterns shown in Figure 2, time-lapse videos of their growth are provided in the ESI†.

The experimental results shown in Figure 2 are supported by numerical simulations using the Lengyel-Epstein model. The results and space-time plots are shown in Figure 3. Notably, the perpendicular stripe pattern in Figure 3c do not show any inverted spot patterns, as the simulations lack any inhomogeneity present in experiments. In addition, the stability of the final patterns was tested using the numerical simulations. As long as a constant light forcing ($W = 1.5$) was used at the edge of the domain, the result-

ing patterns remained stable indefinitely. Time-lapse videos of the simulated pattern development are also provided in the ESI†.

The final pattern morphologies seen in Figures 2 and 3 show good agreement with the one-dimensional axial growth patterns observed by Míguez *et al.*²¹ The concentric rings that are a result of the fast growth rates are the growing circular domain equivalent to the stripes that form parallel to the axial one-dimensional growing boundary. Likewise, for slow growth rates, both the one-dimensional axial growth²¹ and the two-dimensional linear radial growth presented here show patterns forming perpendicular to the growing boundary. We suggest that the parallel-stripe pattern shown in Figures 2b and 3b is the two-dimensional radial growth equivalent to the oblique stripes shown in Ref. 21, as the stripes grow perpendicular to parts of the growing boundary and parallel to other parts. There is fair quantitative agreement between the two-dimensional linear radial growth and Míguez *et al.*'s one-dimensional axial growth,²¹ as the axial growth rates used by Míguez are about twice the radial growth rates in the experiments presented in Figure 2. If we were to consider the growth rate of the diameter of the circular domains, the growth rates in the two works would be similar. This indicates that radial growth in two dimensions is analogous to axial growth in one dimension.

3.2 Growth Modes

In addition to differing final pattern morphologies, we also observe three different Turing pattern growth modes depending on

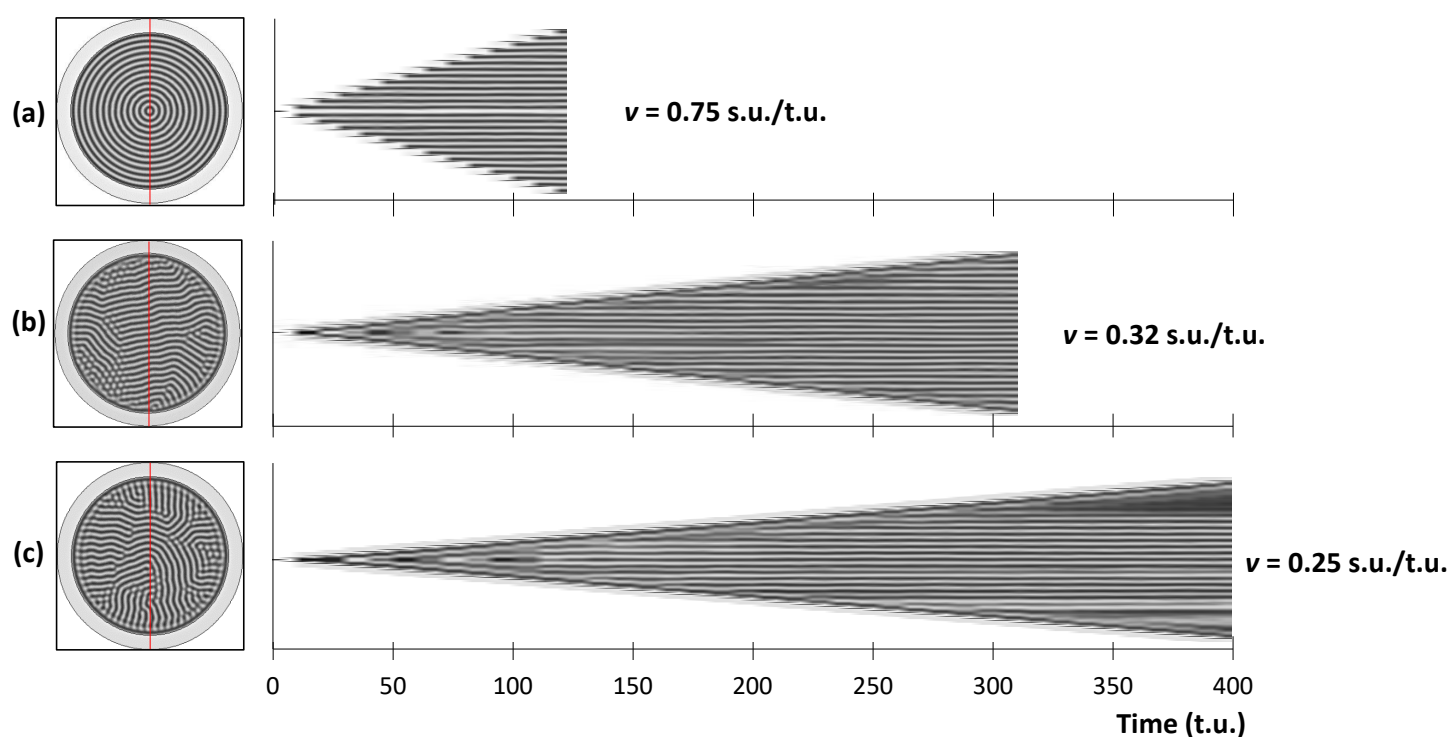


Fig. 3 Simulations of radial growth at fast, intermediate, and slow growth rates for $b = 0.31$. Final Turing patterns (left) are displayed next to the space-time plot of each simulation (right). Each final pattern is image is 115 s.u. across. The red lines indicate where the space-time plot information was taken. Radial growth rates (total growth times) are (a) 0.75 s.u./t.u. (130 t.u.), (b) 0.32 s.u./t.u. (310 t.u.), and (c) 0.25 s.u./t.u. (400 t.u.).

the domain radial growth rate: outer ring addition, perpendicular pattern growth, and inner ring growth. These modes are distinguished by the way in which new wavelengths of the Turing patterns are added to the system. All simulated results presented in the following figures (Figures 4-6) use $b = 0.32$ in Equation 2.

3.2.1 Outer Ring Addition (ORA)

For the experimental conditions described in Section 2.1, the most common of the Turing pattern growth modes is outer ring addition, which occurs for intermediate and faster growth rates. For the ORA growth mode, once an initial spot or stripe forms (Figure 4a) rings are added to the outside of the pattern as the domain grows to accommodate additional wavelengths. In the time-lapse images shown in Figure 4, two rings are added in the experimental images and four rings are added in the simulated images. Space-time plots of images that show the ORA growth mode are characterized by horizontal stripes emerging as the diameter of the growth domain becomes larger, signifying that once the stripe appears it does not shift over time (Figures 2a and 3a).

3.2.2 Perpendicular Pattern Growth (PPG)

The perpendicular pattern growth mode is similar to ORA in the sense that the Turing pattern grows by adding to the outer edge of the existing pattern. However, instead of adding a new stripe, the PPG mode functions by lengthening the existing stripes that are perpendicular (or near-perpendicular) to the growing boundary. This is shown experimentally in Figure 5, where an initial pattern with small perpendicular stripes surrounding a ring (Figure 5a) grows by extending the offshoots, which occasionally

branch into two separate near-perpendicular stripes (Figure 5b-e). If stripes diverge enough for an additional wavelength to fit between them, a new stripe that is perpendicular to the growing boundary emerges. The PPG mode is also shown in simulations in Figure 5. The simulations shown in Figure 5 are of a larger Turing pattern domain to better highlight the growth mode, as for these conditions the simulations begin in a spot pattern before organizing into perpendicular stripes. The spot patterns are temporary, and with time they will resolve themselves into perpendicular stripes. This was confirmed in simulations by stopping the growth while the pattern was spotted. The spot patterns organized into perpendicular stripes after additional time integration at fixed domain size. Space-time plots of patterns that undergo this growth mode are shown in Figure 2c and Figure 3c for experiments and simulations, respectively.

We suggest that the growth mode of the pattern shown in Figures 2b and 3b is a mixture of the ORA and PPG growth modes. Similar to the ORA growth mode, new stripes are added next to the sides of previously formed stripes as the domain grows. However, where the stripes point to the growing boundary, they simply expand their length without any stripe addition as in the PPG mode. This suggestion is supported by the value of the growth rate, which is between the growth rates for PPG and ORA growth modes.

3.2.3 Interior Ring Growth (IRG)

The third Turing pattern growth mode that is observed is interior ring growth (Figure 6). This type of growth only occurs for

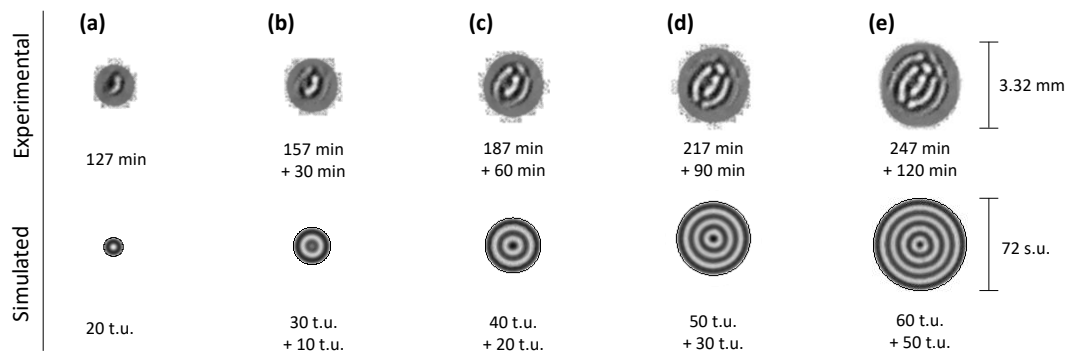


Fig. 4 Time-lapse images of the outer ring addition (ORA) growth mode of Turing pattern development. Experimental domain of Turing patterns grows at a rate of 0.40 mm/h, and the domain of simulated Turing patterns grows at a rate of 0.6 s.u./t.u. The times below each image indicate the time since growth initialization (top) and the time lapsed since the first image in the sequence (bottom).

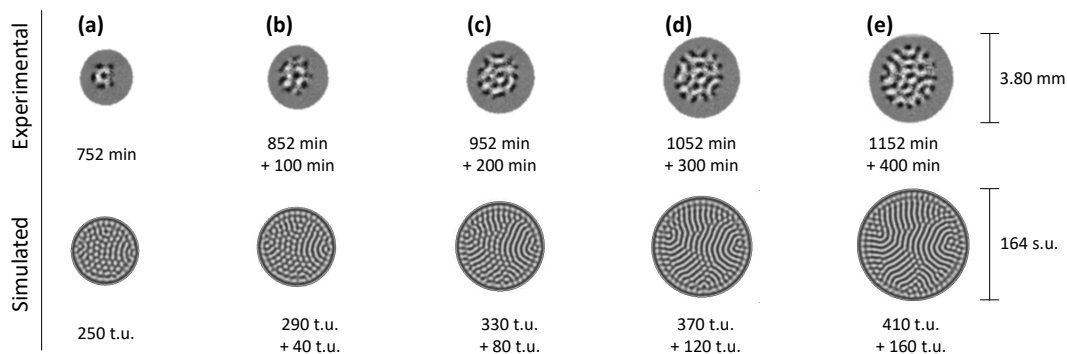


Fig. 5 Time-lapse images of the perpendicular pattern growth (PPG) mode of Turing pattern development. Experimental domain of Turing patterns grows at a rate of 0.10 mm/h, and the domain of simulated Turing patterns grows at a rate of 0.2 s.u./t.u. The times below each image indicate the time since growth initialization (top) and the time lapsed since the first image in the sequence (bottom).

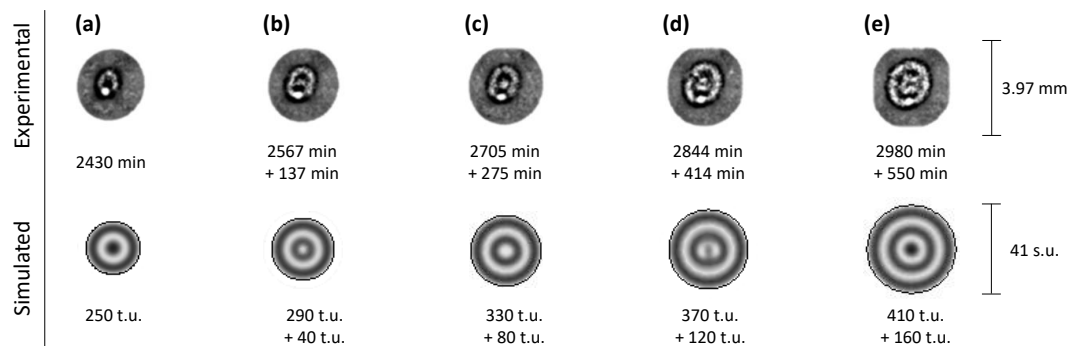


Fig. 6 Time-lapse images of the interior ring growth (IRG) mode of Turing pattern development. Experimental domain of Turing patterns grows at rate of 0.04 mm/h, and the domain of simulated Turing patterns grows at a rate of 0.05 s.u./t.u. The times below each image indicate the time since growth initialization (top) and the time lapsed since the first image in the sequence (bottom).

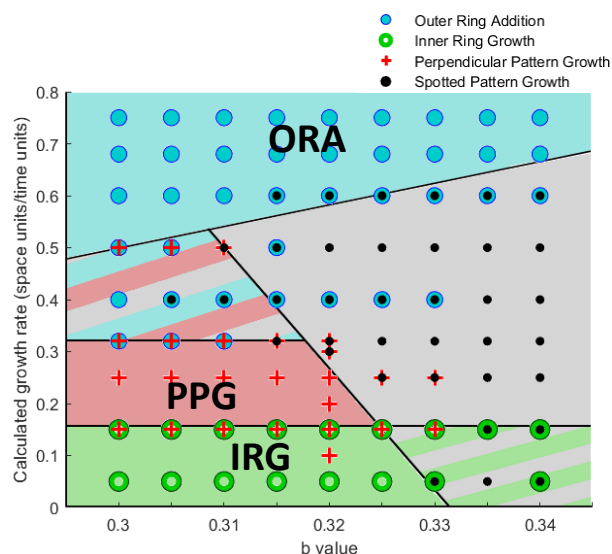


Fig. 7 Parametric diagram of the different growth modes observed in numerical simulations of the Lengyel-Epstein model. All simulated growth was performed until a final radius of 100 s.u. was reached. Symbols are the results of numerical simulations, showing both the final pattern morphology and the growth mode. Mixed modes are shown by two overlapping symbols. Shaded areas are approximate shapes of the different regions in phase space.

extremely slow growth rates, usually below growth rates of 0.05 mm/h in experimental studies. For IRG, due to the slow growth of the non-illuminated area where Turing patterns can arise, the pattern can adjust and grow with the boundary, since the reaction-diffusion dynamics operate on a much faster timescale than the domain growth. The pattern originally starts off as a singular "spot" in the center of the growing domain and then grows into a ring (Figure 6a). As opposed to the ORA growth mode, where each ring within the concentric ring pattern maintains a constant diameter, this ring continues to grow with the boundary. Once there is sufficient space in the middle of the ring, a new spot appears in the center (Figure 6b,c). Both the outer ring and the central spot continue to grow with the outer boundary, until the central spot is large enough to split into a new ring (Figure 6d,e). In this case the wavelength of the Turing pattern changes during the growth in a sawtooth-like manner. First, it increases with the growth until a new spot forms, which results in the wavelength sharply decreasing. This phenomenon may also be seen in the stripe addition of *Pomacanthus semicirculatus*, where the distances between the stripes grow as the fish becomes larger until a new stripe is added between two existing stripes.^{8,25}

3.3 Parametric Diagram and Pattern Robustness

Figure 7 is a parametric diagram showing the growth modes of Turing patterns obtained in simulations with a radially growing two-dimensional domain. The diagram shown is the b (Equation 2)-growth rate plane. We note that the concentric ring morphology arises from both fast and slow growth rates, albeit with different growth modes (IRG for extremely slow growth and ORA

for fast growth). However, the PPG mode appears to be required for the final perpendicular pattern morphology. The patterns that lie close to the boundaries between regions in phase space show transitional behavior that could be interpreted as a mixture of two separate growth modes or final morphologies. Two examples of this are (i) the parallel stripes shown in Figures 2b and 3b and (ii) how the concentric rings formed through the IRG mode shown in Figure 6 eventually break into spots (not shown). The spotted pattern growth region is kept separate because the spots have no spatial orientation. Thus, while they may show the same growth modes as the striped patterns, we cannot classify their orientation as parallel or perpendicular to the boundary in the same way as stripe patterns.

We also see that most regions in the parametric diagram are relatively large, indicating that the behavior of the Turing patterns is robust. This is important in assessing the results of our experiments. Due to the extremely long time scales of most of the experiments, there could be minor fluctuations in initial concentrations of the reagents as they enter the reactor. This may shift the reactor concentrations slightly (within a few percent), but due to the robustness of the patterns in the parametric space diagram we are able to observe the same growth modes in a reproducible manner.

4 Conclusions and Future Work

We have presented here a novel method for studying Turing pattern formation under the condition of two-dimensional linear radial growth. We have shown that both the final pattern morphology and the growth mode of the Turing pattern vary significantly based on the radial growth rate. Specifically, we extend the results of Míguez *et al.* to two-dimensional growth and observe the same pattern orientation trends. Additionally, we observe significant differences in the growth modes of the Turing patterns. To the authors' knowledge, this constitutes the first examination (at least experimentally) of pattern formation on a continuously growing two-dimensional domain. These results are obtained experimentally and supported with data from simulations with the Lengyel-Epstein model. We also present a parametric space diagram to show the impact growth rates have on the growth modes for various b values, and comment on the robustness of the various types of patterns.

Examining the impact of growth on the development of Turing patterns may provide new insight into how patterns, such as animal prints or bird feather patterns, form in biological systems. In particular, this work may guide researchers in biological systems in identifying species that are functionally important in Turing pattern generation based on their concentration profile as the system grows. In addition, this experimental system is highly tunable and can be modified for other types of growth. In the future, we will extend our study to both exponential and logistic growth rates^{26–28}, as well as test the effects of different growing domain geometries on the pattern morphologies. We also plan to experimentally test the conclusions of Klíka and Gaffney²⁸, who claim that growth can be used as a method to initiate Turing patterns under reaction conditions that would not produce a Turing pattern on a static domain. The methods and results in this paper

represent a significant step forward in the study of Turing pattern development, and should lead to a more detailed understanding of how Turing patterns develop in a biological growing system.

5 Conflicts of Interest

There are no conflicts to declare.

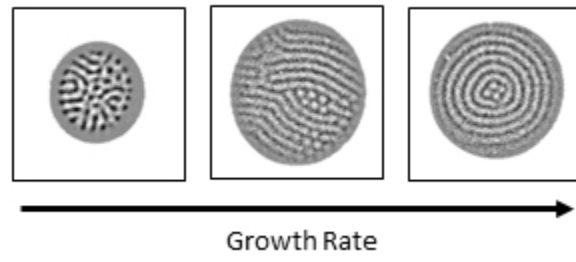
6 Acknowledgements

The authors would like to acknowledge the following individuals: Viktor Hórvath for assistance with the mask generation program and critical equipment repairs and maintenance, Solomon Garber for meaningful discussions and assistance with the image enhancement and analysis programs, and Yunqiao Gan and Tracy Cui for aid in experiment preparation. We also thank the National Science Foundation (NSF CHE-1362477) and the Howard Hughes Medical Institute Exceptional Research Opportunities Program for financial support.

References

- 1 A. M. Turing, *Philosophical Transactions of the Royal Society B: Biological Sciences*, 1952, **237**, 37–72.
- 2 V. Castets, E. Dulos, J. Boissonade and P. De Kepper, *Physical Review Letters*, 1990, **64**, 2953–2956.
- 3 I. Lengyel and I. R. Epstein, *Science*, 1991, **251**, 650–652.
- 4 Q. Ouyang and H. L. Swinney, *Nature*, 1991, **352**, 610–612.
- 5 B. Ermentrout, *Proceedings of the Royal Society A: Mathematical, Physical and Engineering Sciences*, 1991, **434**, 413–417.
- 6 A. Gierer and H. Meinhardt, *Kybernetik*, 1972, **12**, 30–39.
- 7 S. Kondo and T. Miura, *Science (New York, N.Y.)*, 2010, **329**, 1616–20.
- 8 S. Kondo and R. Asai, *Nature*, 1995, **376**, 765–768.
- 9 C. Varea, J. L. Aragón and R. A. Barrio, *Physical Review E*, 1997, **56**, 1250–1253.
- 10 M. P. Harris, S. Williamson, J. F. Fallon, H. Meinhardt and R. O. Prum, *Proceedings of the National Academy of Sciences of the United States of America*, 2005, **102**, 11734–9.
- 11 R. Bailleul, C. D.-T. Dinh, M. Hidalgo, C. Curantz, J. Touboul and M. Manceau, *bioRxiv*, 2018, 491092.
- 12 J. D. Murray, *How the Leopard Gets Its Spots*, 1988.
- 13 R. T. Liu, S. S. Liaw and P. K. Maini, *Physical Review E*, 2006, **74**, 011914.
- 14 E. Meron, E. Gilad, J. von Hardenberg, M. Shachak and Y. Zarmi, *Chaos, Solitons & Fractals*, 2004, **19**, 367–376.
- 15 R. HilleRisLambers, M. Rietkerk, F. v. d. Bosch, H. H. T. Prins and H. d. Kroon, *Ecology*, 2001, **82**, 50–61.
- 16 W. Y. Tam, W. Horsthemke, Z. Noszticzius and H. L. Swinney, *The Journal of Chemical Physics*, 1988, **88**, 3395–3396.
- 17 I. Lengyel and I. R. Epstein, *Proceedings of the National Academy of Sciences of the United States of America*, 1992, **89**, 3977–9.
- 18 J. Horváth, I. Szalai and P. De Kepper, *Science (New York, N.Y.)*, 2009, **324**, 772–5.
- 19 A. P. Muñuzuri, Milos Dolnik, A. M. Zhabotinsky and I. R. Epstein, *Journal of the American Chemical Society*, 1999, **121**, 8065–8069.
- 20 A. Preska Steinberg, I. R. Epstein and M. Dolnik, *The Journal of Physical Chemistry A*, 2014, **118**, 2393–2400.
- 21 D. G. Míguez, M. Dolnik, A. P. Muñuzuri and L. Kramer, *Physical Review Letters*, 2006, **96**, 048304.
- 22 D. K. Gaskins, E. E. Pruc, I. R. Epstein and M. Dolnik, *Physical Review Letters*, 2016, **117**, 056001.
- 23 M. Dolnik, T. Bánsági, S. Ansari, I. Valent and I. R. Epstein, *Physical Chemistry Chemical Physics*, 2011, **13**, 12578.
- 24 D. Feldman, R. Nagao, T. Bánsági Jr., I. R. Epstein and M. Dolnik, *Physical Chemistry Chemical Physics*, 2012, **14**, 6577.
- 25 P. K. Maini, T. E. Woolley, R. E. Baker, E. A. Gaffney and S. S. Lee, *Interface Focus*, 2012, **2**, 487–496.
- 26 A. Madzvamuse, E. A. Gaffney and P. K. Maini, *Journal of Mathematical Biology*, 2010, **61**, 133–164.
- 27 G. Hetzer, A. Madzvamuse and W. Shen, *Discrete and Continuous Dynamical Systems*, 2012, **32**, 3975–4000.
- 28 V. Klika and E. A. Gaffney, *Proceedings of the Royal Society A: Mathematical, Physical and Engineering Science*, 2017, **473**, 20160744.
- 29 *Handbook of Preparative Inorganic Chemistry*, ed. G. Braur and P. G. Stecher, Academic Press Inc., New York, NY, 2nd edn, 1965.

Our study reports three distinct modes of Turing pattern growth, which depend on the radial growth rate of the system.



79x39mm (96 x 96 DPI)